SLAC-PUB-1421
(T/E)
May 1974

MEASUREMENT OF INCLUSIVE HADRON ELECTROPRODUCTION FROM HYDROGEN AND DEUTERIUM*

J. T. Dakin,** G. J. Feldman, F. Martin,
M. L. Perl, W. T. Toner***

Stanford Linear Accelerator Center
Stanford University, Stanford, California 94305

ABSTRACT

We report on the inclusive electroproduction of hadrons from nucleon targets. The incident electron beam energy is 19.5 GeV. We detect scattered electrons corresponding to exchanged virtual photons in the range $-0.25 > q^2 > -3.00$ $(GeV/c)^2$ and $12 < s < 30$ GeV^2. In coincidence we detect most hadrons which go in the forward (virtual photon) direction in the virtual photon-nucleon c. m. system. The cross section for producing these hadrons is studied as a function of azimuthal angle, transverse momentum squared, and a longitudinal momentum related variable. Data are presented for proton, deuteron, and neutron targets, and are largely consistent with the data in real photoproduction ($q^2=0$). Notable differences are that in electroproduction the transverse momentum distributions are somewhat broader, and the forward hadrons are less charge and isospin symmetric. The data are generally consistent with expectations of parton models.

*Work supported by the U. S. Atomic Energy Commission.
**Present address: University of Massachusetts, Amherst, Massachusetts, 01002.
***Present address: Rutherford High Energy Laboratory, Chilton, Didcot, Berkshire, England.

(Submitted to Phys. Rev. D.)

I. Introduction

We report here an experimental study of the final state hadrons produced in inelastic electron-nucleon scattering. It has been observed that the cross section for electron (e) - nucleon (N) scattering where only the final state electron (e') is detected,

$$eN \rightarrow e' + \text{hadrons} \qquad (1)$$

exhibits a remarkable kinematic regularity which we will refer to as "leptonic scaling"[1] (to differentiate it from scaling in the hadronic final states, which we will discuss later). By investigating the single hadrons (h) ejected in coincidence with electrons,

$$eN \rightarrow e'h + \text{anything}, \qquad (2)$$

we hope to gain insight into the physics underlying leptonic scaling. Brief accounts of this investigation have been reported earlier.[2] In addition to the inclusive reaction (2) considered here, we have also reported a study of the exclusive channels $ep \rightarrow ep\rho^{o}$ and $ep \rightarrow ep\varphi$.[3]

In the remainder of this section we will discuss A., definitions of kinematic quantities and cross sections; B., the scope of the experiment; C., pertinent theoretical ideas; and D., other experiments. In Section II the apparatus will be described. In Section III we will tell how the data was reduced to final cross sections and parameters. Section IV will contain a presentation and discussion of results, and Section V will contain conclusions.

A. Kinematics and Definitions

To first order in quantum electrodynamics reactions (1) and (2) proceed via single photon exchange, as indicated in Fig. 1. One can represent them as two-step processes. First, the electron is scattered producing a virtual photon

$$e \rightarrow e'\gamma^{*} . \qquad (3)$$

Second, a virtual photoproduction interaction takes place

$$\gamma^*N \rightarrow \text{ hadrons}, \tag{4}$$

or

$$\gamma^*N \rightarrow h + \text{anything}. \tag{5}$$

Reaction (3) can be described by 3 independent kinematic variables: q^2, the square of the four-momentum carried by the virtual photon; ϵ, the photon polarization parameter; and s, the square of the total energy in the γ^*N collision as measured in the γ^*N center-of-mass system. In terms of the incident and scattered electron energies in the laboratory, E and E', the electron scattering angle in the laboratory, θ, and the nucleon mass, m, these variables can be expressed as

$$q^2 = -4EE' \sin^2(\theta/2) \tag{6.1}$$

$$s = m^2 + 2(E-E')m + q^2 \tag{6.2}$$

$$\epsilon = [1 + 2(1 - (E-E')^2/q^2) \tan^2(\theta/2)]^{-1}. \tag{6.3}$$

Throughout this discussion the electron mass is neglected, and we consider only unpolarized electron beams and unpolarized targets.

It is customary to define $\sigma_{tot}(q^2, s)$, the cross section for reaction (4) at a given q^2 and s. This is done by assigning a flux, Γ, to the virtual photons in reaction (3)[4]

$$\Gamma = \frac{\alpha}{8\pi} \frac{s - m^2}{m^2E^2(-q^2)(1-\epsilon)} \tag{7}$$

and then writing

$$\sigma_{tot}(q^2, s) = \frac{1}{\Gamma} \frac{d\sigma}{dq^2 ds} \quad , \tag{8}$$

where $d\sigma/dq^2ds$ is the differential cross section for reaction (1). We have not mentioned the variable ϵ because in our experiment with fixed incident electron energy, q^2 and s determine ϵ uniquely.

Inclusive virtual photoproduction, reaction (5), is considered in its center-of-mass frame, where three kinematic variables for the final hadron are defined relative to the incident γ^* direction. The hadron azimuthal angle, φ, is measured relative the the electron scattering plane — the transverse polarization plane of the γ^*. The square of the transverse

momentum is denoted $p_\perp^2$. The dimensionless variable x is the longitudinal component of the hadron momentum divided by p^*_{max}, the maximum possible pion momentum from a γ^*N interaction at the same s.[5]

Using these variables one can define the virtual photoproduction differential cross section at a given combination of q^2 and s in terms of the cross section for reaction (2):

$$\frac{d\sigma(q^2,s)}{dp_\perp^2\, d\varphi\, dx} = \frac{1}{\Gamma} \frac{d\sigma}{dp_\perp^2\, d\varphi\, dx\, dq^2\, ds} \quad . \tag{9}$$

It is, however, more convenient to take the ratio of equations (9) and (8), and normalize the differential to the total cross section, giving the quantity

$$\frac{1}{\sigma_{tot}(q^2,\, s)} \frac{d\sigma(q^2,s)}{dp_\perp^2\, d\varphi\, dx} \quad .$$

Here the somewhat arbitrary flux factor, Γ, has cancelled and one is left with an expression whose normalization is easily understood. Furthermore it is an expression which is easily determined experimentally. It is the ratio of the cross sections for reactions (2) and (1) — the number of scattered electrons in a given $(q^2,\, s)$ interval divided into the number of those electrons which are coincident with hadrons in a given $(p_\perp^2, \varphi, x)$ interval.

Two projections of the differential cross section will be used to present the data. Both involve integrals over the variables φ and $p_\perp^2$. For the first, the cross section is converted to the Lorentz-invariant form

$$\frac{1}{\sigma} E \frac{d^3\sigma}{dp^3} = \frac{2E^*}{p^*_{max}} \frac{d\sigma(q^2,s)}{dp_\perp^2 d\varphi\, dx} \frac{1}{\sigma_{tot}(q^2,s)} \tag{10}$$

where E^* is the hadron energy in the virtual photoproduction center-of-mass system. This expression is then integrated over $p_\perp^2$ and averaged over φ to give the structure function which is common in the literature,

$$f(x) = \int_0^{2\pi} d\varphi \int_0^{\infty} dp_\perp^2 \frac{1}{\pi} \frac{E^*}{p^*_{max}} \frac{d\sigma(q^2,s)}{dp_\perp^2\, d\varphi\, dx} \frac{1}{\sigma_{tot}(q^2,s)} \quad . \tag{11}$$

The second projection of the cross section is the differential multiplicity, which represents the number of hadrons per increment in x

$$\frac{dN}{dx} = \int_0^{2\pi} d\varphi \int_0^{\infty} dp_\perp^2 \; \frac{d\sigma(q^2,s)}{dp_\perp^2 \, d\varphi \, dx} \; \frac{1}{\sigma_{tot}(q^2,s)} \quad . \tag{12}$$

In extracting the structure function and the differential multiplicity we assume that the $p_\perp^2$ and φ dependence of the cross section can be expressed as

$$\frac{d\sigma}{dp_\perp^2 \, d\varphi \, dx} \propto e^{-bp_\perp^2} \, (1 + A \cos\varphi + B \cos 2\varphi) \quad . \tag{13}$$

This is a weaker assumption than that of factorization in $p_\perp^2$, φ and x because here the parameters b, A and B can depend on x. In a preliminary study of the data we have verified that equation (13) is an accurate parameterization of the $p_\perp^2$ and φ dependences of the cross section.[6] The φ dependence is, in fact, the most general dependence allowed for single photon exchange (Fig. 1). Here the cos 2φ term reflects any polarization dependence of the cross section for transversely polarized virtual photons. The cos φ term reflects any interference between the longitudinal and transverse virtual photon scattering amplitudes.

B. Experimental Scope

The kinematic range over which this experiment has data is summarized in Table I. The significance of the q^2 - s range can be seen by noting that leptonic scaling in reaction (1) occurs for $s > 4$ GeV^2, and $|q^2| > 1$(GeV/c^2)[1] Here $s > 12$ GeV^2 places the data well away from the resonance region ($s < 4$ GeV^2), where the hadronic final states are dominated by baryonic resonances. The q^2 region of this data therefore covers the transition region between real photoproduction ($q^2 = 0$), and full leptonic scaling. The incident beam energy is fixed at E = 19.5 GeV, hence the polarization varies from $\epsilon \sim 0.4$ at $s = 30$ GeV^2 to $\epsilon \sim 0.9$ at $s = 12$ GeV^2.

The final state hadrons are those in the forward direction in the γ^*N c.m.

frame. In diffractive models for γ^*N interactions this region is populated by the decay products of the photon. In parton models this region is populated by the struck parton after it is dressed. In either case, this region is generally referred to as the photon or current fragmentation region.

Data were collected both with hydrogen (H_2) and with deuterium (D_2) targets. Hence we were able to extract data for γ^*n as well as γ^*p interactions. The final-state hadrons observed were both positive (h^+) and negative (h^-). While there was no means for π-K-p separation, we deduce from experiments in nearby kinematic regions that the hadrons are predominantly π's.

C. Theoretical Guidelines

Since the discovery of leptonic scaling in reaction (1) a considerable amount of theoretical work has been done on electroproduction.[7] A comprehensive review of this work is well outside the scope of this paper. Here we will present instead an outline of those theoretical predictions and questions which are pertinent to our data.

1. φ dependence

Because the γ^*'s are polarized both transversely and longitudinally, non-zero values of A and B are allowed. A general prediction of the parton model, however, has been that such terms should decrease with increasing $|q^2|$.[8]

2. $p_\perp^2$ dependence

It has been hypothesized that as $|q^2|$ increases and the virtual photon gets further from the mass shell its effective size when interacting with a hadron should shrink.[9] This should lead to a growth in the average $p_\perp^2$ in reaction (5), or equivalently to a decrease in b.[10,11]

3. Hadronic scaling

An important prediction[12] of the parton model is that the Lorentz invarient cross section given in equation (10) should be independent of s at fixed ω, where

$$\omega = (q^2 + m^2 - s)/q^2 \quad . \tag{14}$$

Since hadronic scaling of this sort implies that the $p_\perp^2$ dependence of this invariant cross section is independent of q^2 for fixed ω and x, this scaling requires scaling in the structure function $f(x)$.

4. Inclusive - exclusive connection

Bjorken and Kogut have argued on general grounds that the shape of the structure function near $x = 1$ should be related to the Regge intercepts of exchanged particles and to the asymptotic fall off of elastic and transition form factors.[13] In particular it is expected that $f(x) \propto (1-x)$ corresponding to a pion form factor falling asymptotically as $(-q^2)^{-1}$.

5. π^+/π^- ratios

For a given x interval (x_1, x_2) in the photon fragmentation region we define the partial multiplicities $N^+(N^-)$ for positive (negative) pions:

$$N^\pm = \int_{x_1}^{x_2} dx \, \frac{dN^\pm}{dx} \quad . \tag{15}$$

Then we can define the particle ratio

$$R = N^+/N^- \quad . \tag{16}$$

If γ^*N interactions have the diffractive character which one might expect from analogy to strong interactions at large s, then one would expect $R = 1$ since the photon is neutral.[14] This is also what one expects in the vector dominance model if the vector meson-nucleon interaction is diffractive. It has, however, been pointed out that the vector meson-nucleon interaction could have a non-diffractive part which grows with $|q^2|$ and produces $R \neq 1$.[15]

In the quark-parton model one expects more specific charge assymetries due to the photon's four times greater preference striking a u-type (charge + 2/3) than a d-type (charge - 1/3) quark. In the most naive model one expects $R = 8$ for a proton target, and $R = 2$ for a neutron target.[16] In more sophisticated models one expects these ratios to be diluted, and ω-dependent, but still greater than 1 when the appropriate ω-average is taken.[17,18] These latter models give the ω dependence of R for both the proton and the neutron after

just one free parameter is determined — the relative probabilities for a u-type quark to dress as π^+ and π^-.

Another prediction of the quark-parton model, with no free parameters, is the sum rule for electroproduced π's [19]

$$\frac{\int_1^\infty (N_n^+ - N_n^-)\, F_{1n}(\omega)\, \frac{d\omega}{\omega^2}}{\int_1^\infty (N_p^+ - N_p^-)\, F_{1p}(\omega)\, \frac{d\omega}{\omega^2}} = \frac{2}{7} \quad . \tag{17}$$

Here the subscript p (n) denotes proton (neutron) target, and the F_1's are standard nucleon structure functions.[1]

6. Parton Charge

Feynman has conjectured that one can measure the quantum numbers of the average struck parton by observing the average quantum numbers of hadrons in the parton fragmentation region.[20] One might test this by seeing whether the average charge $(N^+ - N^-)$ is consistent with the average struck parton charge that one expects in a given parton model for the proton.[21] Such a test, however, involves two difficulties. At our non-asymptotic values of s there is no neutral central plateau in rapidity, and it is not obvious what x_1, x_2 interval to take for the integral in expresssion (15). Second, there are examples of specific models where Feynman's conjecture does not hold.[22,23]

D. Other experiments

A number of other groups have studied the inclusive electroproduction of hadrons. Because the results of their experiments will be referred to often in the text, we will review here briefly their experimental scopes. Most of these experiments explore the q^2 - s range which, like ours, can be characterized as the transition region between photoproduction and leptonic scaling. The most important differences between the experiments involve their x - $p_\perp^2$ - φ regions.

Two groups have used triggered 4π detectors which are sensitive to the entire $x - p_\perp^2 - \Phi$ space. One used a streamer chamber in a 7.2 GeV/c electron beam at DESY.[24] The other used hybrid bubble chamber techniques in a 16 GeV/c muon beam at SLAC.[25] The DESY group has reported primarily π^- inclusive spectra. The SLAC group has used ionization and kinematic constraint information to obtain π^+ and p inclusive spectra in addition to the π^- spectrum.

All of the remaining four groups have used two-arm spectrometers, where one arm detects a scattered electron and the other a hadron. Two groups at DESY have explored the forward region, $x > 0$, and have had Cerenkov counters in their hadron spectrometers to give π-K-p separation. One of these groups has reported only the π^+ and π^- spectra over the relatively low q^2 range $-0.1 > q^2 > -0.7 (\text{GeV/c})^2$.[26] The other group[27] has presented p, π^+, π^-, K^+ and K^- spectra at $q^2 = 1.16 (\text{GeV/c})^2$.

Two groups at Cornell have used 2-arm spectrometer systems which are quite complimentary to one another. The first[28-30] has explored hadrons with $x > 0$ using a Cerenkov counter for π - K - P separation. The second[31] has explored hadrons with $x < 0$ using time-of-flight techniques for π-P separation.

Only one other group[28] has reported results from a deuterium target.

II APPARATUS

The experiment was done at the Stanford Linear Accelerator Center (SLAC). The apparatus consisted of a 19.5 GeV electron beam incident on a 4 cm liquid hydrogen target and a large aperture spectrometer to detect a large fraction of the forward final state particles with lab momenta greater than $\sim$1 GeV/c. These elements are shown in Fig. 2 and discussed in greater detail below.

The electron beam contained typically 10^4 e^- per 1.5μsec long SLAC pulse. At the experimental target, the beam had an rms width of 0.5 mm x 0.5 mm and an rms divergence of less than 0.2 mrad x 0.2 mrad. There the beam was very well collimated, with fewer than 1 in 10^5 e^- outside a 0.5 cm diameter circle. The momentum spread in the beam was 0.2%.

The target was a 4 cm long flask which was filled with either liquid H_2 or liquid D_2 or left empty to determine target wall backgrounds.

The spectrometer magnet had 1.37 m diameter pole faces separated by 0.91 m. It was centered on the beam line, 2.54 m downstream from the target, with its principal field component horizontal. At the magnet center, this field was 10 kG and the field integral 17 kG-meters. The unscattered beam and the forward electromagnetic backgrounds passed through the magnet in a field-free region created by a cylindrical superconducting tube.[32] Beyond the magnet were two optical spark chambers separated by 1.7 m. The chambers had inactive holes through their centers, where the beam tube passed. The apertures of the magnet, spark chambers, and beam tube produced the acceptance shown in Fig. 3.

The apparatus was triggered on the detection of a scattered electron by a hodoscope of 20 scintillation counters and 11 shower counters[33] behind the second spark chamber. The shower counter thresholds were set to $\sim$4 GeV. Photon triggers were eliminated by the requirement that a shower counter fire coincident with one of the scintillators in front of it. The kinematic range of inelastic electron scattering covered by this trigger was roughly $|q^2| > 0.3$ (GeV/c)^2, $s < 30$ GeV^2. There was no hadron requirement in the trigger.

For each trigger a single picture was taken of the optical spark chambers on 70 mm film. The camera was located in the horizontal plane 21.6 m from the beam line with its optic axis aligned perpendicular to the beam. Each picture contained four views of each chamber, a direct view, a top and a bottom view in small angle stereo, and a rear view to expose tracks blocked in the direct view by a beam pipe.

The apparatus included no capability for distinguishing between pions, kaons and protons.

A PDP-8 computer recorded scintillation and shower counter status, shower counter pulse heights, and scintillation counter timing information for each event.

The beam flux was integrated by a quantameter located behind the shower counters and was monitored instantaneously by a surface-barrier detector.[34]

III Data Reduction

We recorded 2.5 X 10^5 triggers with the H_2 target and 1.1 X 10^5 triggers with the D_2 target. These data samples contained integrated fluxes of 2.6 X 10^{12} and 0.7 X 10^{12} incident electrons respectively, as summarized in Table II. Below we will describe the following steps for reducing these data samples to cross sections: A, event identification and reconstruction; B, the internal normalization to reaction (1); C, the fitting procedure to determine b, A, B, f(x) and dN/dX for reaction (2); D, the deuterium subtraction; and E, other data which suggest that our hadrons are mostly pions.

A. Event Reconstruction

All of the film was measured by a flying-spot digitizer, Hummingbird II,[35] to find events which were candidates for reaction (1) or for reaction (2). First each event was searched for straight tracks in the spark chambers. The momentum of each such track was computed by propagating the track back through the magnet while adjusting the momentum to make the track strike the target vertically. If, after this momentum optimization, the track did not project back to the target in the horizontal (non-bending) plane, it was rejected. The rms momentum resolution was 2% at 10 GeV/c.

A track was interpreted as an electron (e') if its direction of bend corresponded to negative charge, and its momentum was consistent with the pulse height in the shower counter through which the track passed. All other tracks were interpreted as hadrons (h). Both hadron and electron tracks were required to be consistent with the latch and timing information in the scintillator hodoscope.

Each detected e' was interpreted as one event of reaction (1) or (4), for which the variables q^2 and s were computed. Each coincident combination of an e' and a h was interpreted as one event of reaction (2) or (5). (When more than one h were found in one picture, each was paired separately with the e' to make a separate e'h event.) The variables $p_\perp^2$, φ and x were computed for each e'h event. In making the Lorentz transformation necessary in calculating x, the h was assumed to have the π mass. Within the kinematic limits described in Table I the number of e' and e'h events in each of the data samples is indicated in Table II.

To study the efficiency and possible biases of the flying-spot digitizer

we measured 2.8 X 10^4 frames of H_2 data and 4.7 X 10^3 frames of D_2 data with a highly efficient manual system. This gave the efficiencies shown in Table III for finding e' and e'h events in the film. We could find no evidence of biases introduced by these inefficiencies. The estimated uncertainty in these inefficiencies contributes an over all normalization uncertainty of $\pm$ 20% to the final cross sections.

B. Normalization to Scattered Electrons

Each e' event was placed in one of 12 bins in the q^2 - s plane. The H_2 and D_2 samples were binned separately. Here we describe how the number of e' events in each q^2 - s bin was corrected to obtain $N^e(q^2, s)$, the total number of γ*N interactions in either data sample. The 12 bins formed a 3 x 4 grid in q^2 and s. There were 3 ranges in s (12 to 18, 18 to 24 and 24 to 30 GeV^2) and 4 ranges in q^2 (-0.25 to -0.5, -0.5 to -1.0, -1.0 to -2.0, and -2.0 to -3.0 $(GeV/c)^2$.

Each number was divided by the scanning-measuring efficiency given in Table III.

Each number was divided by the geometric efficiency for detecting an electron, which was determined by a Monte Carlo integration over the apparatus apertures. This efficiency was different for each q^2 - s bin, varying from 0.22 in the worst bin to 0.96 in the best bin.

A radiative-correction factor was applied to each number to convert to the number of non-radiative e' events in the bin.[36] This factor was different for each q^2 - s bin, varying from 0.54 at low $|q^2|$ and high s to 0.91 at high $|q^2|$ and low s. Separate corrections were applied to the H_2 and to the D_2 samples. The radiative effects were found to be dominated by an influx of events from the radiative tail of elastic eN scattering.

A hadron contamination was subtracted from each number. This contamination was estimated by counting the number of tracks which met the electron criteria, but with positive charge. Tracks of this type were assumed to be either positive hadrons or positrons. In either case an equal number of

negative tracks was assumed to exist as a contamination to the true scattered electrons. This contamination varied from 6% at high s to 0.5 % at low s.

C. Fits for Inclusive Cross Sections

Each e'h event was in the 6-dimensional space q^2 - s - $p_\perp^2$ - $|\varphi|$ - x - charge. The 6-dimensional distribution of all events, which we will refer to as N_6, was fitted to determine the parameters b, A, B, and the projected cross sections f(x) and $\frac{dN}{dx}$. The 6-dimensional distribution was binned in the same q^2-s bins as the single electron distribution. In the remaining variables the binning was $p_\perp^2$, 7 bins of width 0.1 $(GeV/c)^{-2}$; $|\varphi|$, 6 bins of width $\pi/6$; x, 6 bins of width 0.15; and charge, 2 bins.

A fit was done for a given hadron charge (+ or-), a given data sample (H_2 or D_2), and a given range in q^2, s and x. Within this range the 6-dimensional distribution was assumed to be represented either as

$$N_6 = \frac{f(x)}{\frac{1}{\pi}\frac{E^*}{p^*_{max}}} \cdot N^e(q^2,s) \cdot b\, e^{-bp_\perp^2} (1 + A\cos|\varphi| + B\cos|2\varphi| \cdot \frac{W}{\pi} \cdot G_6 \qquad (18)$$

or as

$$N_6 = \frac{dN}{dx} \cdot N^e(q^2,s) \cdot b\, e^{-bp_\perp^2} (1 + A\cos|\varphi| + B\cos|2\varphi|) \cdot \frac{W}{\pi} \cdot G_6 \qquad (19)$$

Here W represents the product of the ϕ, $p_\perp^2$, and x bin widths, and G_6 represents the 6-dimensional geometric efficiency which was computed by a Monte Carlo program. Note that we use the variable $|\varphi|$ rather than φ to take advantage of an assumed symmetry in the data, and thereby reduce the number of bins.

When fitting with either expression (18) or expression (19) b, A and B were varied to find the combination which gave the maximum likelihood of observing the distribution N_6. Then the projected cross section f(x) or dN/dx was chosen to make the observed number of events match the expected number of events. The errors quoted for all of these quantities are statistical, and have the normal standard deviation interpretation. In quoting the error in a given quantity determined by a fit (e.g. dN/dx) we fold in the effects of uncertainty of other quantities determined by the fit (e.g. b or A).

Included in the computations of dN/dx and f(x) was a small correction for effects of e'h events where the e' was a misidentified hadron, and

and for $e'h^-$ events where we could not determine which negative track was the hadron. These corrections were always less than 4%.

In addition to the procedure described here we had an analogous procedure in which N^e was binned in ω and s, and N_6 was binned in ω, s, $p_\perp^2$, $|\varphi|$, x and charge. Here the 4 q^2 bins were replaced with 4 ω bins (3 to 10, 10 to 20, 20 to 35, and 35 to 60). When we refer to data in some range of ω, the data were extracted using this procedure.

The only correction made for radiative effects is the correction to the normalization discussed earlier. We estimate that the omitted corrections do not have an important effect on the shapes of the x, $p_\perp^2$, and φ distributions or the charge ratios. However they shift the normalization and cause us to observe cross sections which are too small by approximately 10%.

D. Deuterium Subtraction

To extract values of dN/dx and f(x) for γ^*n interactions we assumed that a deuteron acts as the simple sum of a proton and a neutron. This assumption says, for instance, that

$$\sigma^d_{tot(q^2,s)} = \sigma^p_{tot(q^2,s)} + \sigma^n_{tot(q^2,s)} , \qquad (20)$$

where d, p, and n denote deuteron, proton, and neutron cross sections respectively. One effect which might cause this relationship to break down is "shadowing", which would make the deuteron cross section smaller reflecting the ability of one nucleon to hide behind the other. We know, however, that in the q^2 - s range of our experiment shadowing is negligible even in very heavy nuclei.[I] Another aspect of shadowing is that after an interaction takes place on one nucleon, the produced hadrons could have a secondary interaction on the remaining nucleon. We estimate that this is a small effect. Another effect which might cause trouble is the "smearing" of features in the proton and neutron cross sections by the Fermi motion of the deuteron. This effect, too, is negligible in our region of q^2 and s.[37]

For our purpose the additivity assumption was applied in the form

$$\frac{dN_n}{dx} = \frac{\sigma^d_{tot(q^2,s)}}{\sigma^n_{tot(q^2,s)}} \frac{dN_d}{dx} - \frac{\sigma^p_{tot(q^2,s)}}{\sigma^n_{tot(q^2,s)}} \frac{dN_p}{dx} , \qquad (21)$$

or its equivalent for f(x). The ω-dependent $\sigma^p_{tot}/\sigma^n_{tot}$ ratio was taken[38] to be

$$\frac{\sigma^p_{tot(q^2,s)}}{\sigma^n_{tot(q^2,s)}} = 1.04 \frac{\omega}{\omega-1} \qquad (22)$$

and $\sigma^d_{tot}/\sigma^n_{tot}$ was computed with relationship (20). A slightly more complicated formula than equation (21) was actually used which included corrections for the effects of a 3% hydrogen contamination in the deuterium, and target-wall events which made up 4% of the deuterium sample and 8% of the hydrogen sample.

E. Hadron Classification

The experiment has given us no information as to whether the hadrons are pions, kaons, or protons. When interpreting some aspects of the data, however, it will be valuable to know which type of particle is dominant, and what contaminations from other types are present. Here we will present evidence that the hadrons are predominantly pions.

We will consider the h^+ spectrum. It is likely from quantum number considerations that the p and K^+ contaminations are relatively larger here than the $\bar{p}$ and K^- contaminations in the h^- spectrum. The dN/dx spectrum for h^+ over the interval $12 < s < 30$ GeV^2, $-0.5 > q^2 > -3.0$ (GeV/c)^2 is shown in Table IV. This spectrum is typical of our data.

The proton contribution can be estimated by extrapolating either from electroproduction measurements at comparable values of q^2 but lower values of s, or from photoproduction measurements at comparable values of s but $q^2 = 0$. A Cornell experiment has measured the forward electroproduction of protons at $s = 7.3$ GeV^2 and at several values of q^2.[29] That experiment indicates that the proton structure function does not change significantly with q^2; photoproduction data are consistent with electroproduction data at $q^2 = -2$(GeV/c)^2. However, the proton structure function appears to decrease rapidly with increasing s, roughly as s^{-3}.

Photoproduction experiments at Desy[39] and SLAC[40] span our region of s and indicate a forward proton structure function approximately half the size of that measured in the Cornell electroproduction experiment.

If we assume that there is also no q^2 dependence in the proton structure function in our region of s, then the "proton contamination" shown in Table IV would result. The contamination varies from 10% of the observed hadrons at low x to 5% at high x. (Note that Table IV does not give an estimate of the proton partial multiplicity, but rather of partial multiplicity of protons misidentified as pions. These quantities differ because the Lorentz transformation depends on the particle's mass. For example, at $q^2 = -1$(GeV/c)^2 and $s = 12$ GeV^2, a proton with $x = 0.23$ is interpreted as a pion with $x = 0.40$.)

To estimate the kaon contamination from the Cornell data[30] is more difficult because at $s = 7.3\ GeV^2$ the K^+ spectrum is dominated by K^+ — hyperon exclusive channels which are known to fall rapidly as s increases. In photoproduction data in our s range[39,40] K^+/π^+ ratios range from 10% to 16% and K^-/π^- ratios range from 2% to 8%.

As these estimates are purely extrapolations, we make no corrections for the K and p contaminations, and continue to refer to the data as hadron rather than pion data.

IV Results and Discussion

In this section we will present data tables and figures based on fits to the data. The selection of material, and even more so the discussion is addressed to the questions outlined in Section I.C. In presenting numbers in the tables we will tell whether the target is proton (p), deuteron (d) or subtracted neutron (n); whether the observed hadron is positive (h^+) or negative (h^-); and the q^2, s and x range included in the fit. The errors shown are statistical only. We estimate that the over all normalization error could be as large as 20%, and that h^+/h^- normalization errors are no larger than 10% for the p target or 20% for the n target.

A. φ Distributions

In Tables V and VI are the b,A and B parameters resulting from fits to equation (19). In Table V the fits are done for two broad x regions and for small bands in q^2 and s. In Table VI the fits are done for all 6 x bins and for a large region in q^2-s. While there is evidence for deviations from a uniform φ distribution, there is no particularly striking pattern to this deviation.

The data are consistent with the following trend: $A = B = 0 \pm 0.1$ for $x < 0.4$, and $A=B=0.1 \pm 0.1$ for $x > 0.4$. The transverse polarization (B) effect is quantitatively consistent with the effect seen with real polarized photons at $s = 18$ GeV^2.[41] Our data cannot tell us, however, whether the polarization effects are rising or falling with $|q^2|$. Somewhat larger polarization effects have been seen in inclusive π^- electroproduction at lower s.[24]

As a convenience in analysis we have set $A = B = 0$ for the fits presented from Table VII on. Because the coupling from A and B to the other quantities (b, f(x) and dN/dx) is negligible this introduces no bias in the later results.

B. $p_\perp^2$ Distributions

Values for the parameter b are also available in Tables V and VI. Note that these b values are slightly different than would be the values obtained by fitting to equation (18), where $p_\perp^2$ dependence is introduced by the E* term, particularly at low x.

The q^2- dependence of the b's from Table V is shown in Fig. 4. Included at $q^2 = 0$ are values from the photoproduction of π^- at s = 18 GeV^2.[41] These were obtained by re-fitting the data in Ref. 41 to account for the E* effect mentioned above. In the high x region the b's tend to decrease with increasing q^2, consistent with the shrinking photon hypothesis.

The x-dependence of the b's from Table VI is shown in Fig. 5. There one can see a tendancy for the b's to decrease as the hadrons become more forward. The increase in b in the highest x bin possibly reflects the effect of the edge of phase space. There is no significant difference between the b's from the p target and those from the d target.

C. Projected Cross Sections

The invariant structure function, f(x), and the differential multiplicity, dN/dx, obtained from fits to equations (18) and (19) are presented in Tables VII, VIII and IX. Note that the parameters A and B were set to 0 for these fits. The parameters b obtained from these fits are not shown, but are consistent with those discussed above.

The structure functions for producing h^+ and h^- from the proton and from the neutron for the range $-0.5 > q^2 > -1.0$ $(Gev/c)^2$ and $12 < s < 30$ GeV^2 are shown in Figure 6. These spectra are typical of all of the data. All four spectra have similar shapes, the principal differences being normalization differences. At all values of x there is more h^+ than h^- from the proton target. There is more h^- than h^+ from the neutron target at low x, but more h^+ at higher x.

The errors are considerably larger for the neutron spectrum because there is relatively little deuterium data (see Table II) and the statistical errors are magnified in the deuterium subtraction. The proton data in Fig. 6 is also shown in Fig. 7 on a linear scale.

Some typical differential multiplicity data from the proton target are shown in Fig. 8a. Here one can see directly how the particles are distributed in x; there are very few particles at high x. The difference between the h^+ spectrum and h^- spectra is plotted in Fig. 8b. The area of this gives the charge per event with $x > 0.1$. For the kinematic region included ($-0.5 > q^2 > -3.0$ (GeV/c)^2, $12 < s < 30$ GeV^2) this integral is 0.33, just a fraction of the net charge of +1 required in a γ^*p final state. Here one sees immediately the difficulty of measuring the charge in the current fragmentation region. This charge is very sensitive to the x limit which one uses to define the lower edge of this region. The particle ratio is plotted as a function of x in Fig. 8c. Here the ratio is $\sim$ 1.75 at high x, and somewhat lower at low x. A similar x dependence has been seen in a spectrometer experiment at Cornell.[28]

In Fig. 9 the hypothesis of hadronic scaling is tested. We plot the structure functions for the proton target for a fixed ω interval ($10 < \omega < 35$) in three different s regions. The h^+ distributions fall on top of each other, as do the h^-, which is consistent with scaling. A similar observation of scaling has been made in an experiment at Cornell.[28]

The spectra which we observe are very similar to the spectra observed in other photoproduction and electroproduction experiments. This is seen in Fig. 10 where representative data from several measurements of $\gamma^*p \to \pi^-$ anything are plotted together. The effect of the quasi-elastic channel $\gamma^*p \to \rho^o p$ has been removed from the photoproduction data of Moffeit et al.[41]; the agreement would be much worse around $x \sim 0.6$ if the π's from ρ^o decay were included. (We know that this channel makes a major contribution at

$q^2 = 0$, and a much smaller contribution above $|q^2| = 0.5$ $(GeV/c)^2$. [3] For one of the experiments shown the structure function $f(x)$ is not reported.[28] To present representative data for that experiment we did an integral over $p_\perp^2$ by assuming an $e^{-6p_\perp^2}$ dependence in the Lorentz-invariant cross section.

D. Particle Multiplicities and Ratios

When the $f(x)$ and dN/dx spectra are studied as functions of q^2 and s or ω and s the most significant changes are changes in normalization rather than changes in shape. Hence these changes are most easily presented in terms of the integrals of these spectra. Because of its straightforward interpretation as the number of particles per event in a given x range, we have chosen to work with the partial multiplicity defined in equation (15). Values of N_p^+, N_p^-, N_n^+ and N_n^- are given as functions of q^2, s and ω in Table X. We have presented these x integrals over two x regions. The region $0.1 < x < 1.0$ is the maximum span of our data. The region $0.4 < x < 0.85$ is chosen to be safely within the photon fragmentation region, but not to include the region $x > 0.85$ which has large contributions from exclusive channels such as $\gamma^* p \to \pi^+ n$ While the inclusion of $x > 0.85$ would have little effect on our data, it would confuse the comparison with data at lower s, where these exclusive channels provide a considerably larger fraction of the cross section.

The most dramatic effect in this data is the change in the relative numbers of positive and negative hadrons with q^2 and ω. This can be seen in Figs. 11 and 12 where we plot N_p^+/N_p^- and N_n^+/N_n^- as functions of q^2 and ω for $0.4 < x < 0.85$. Included on these plots are representative

data from other experiments which have reported the π^+/π^- ratio in similar x ranges. In photoproduction ($q^2 = 0$, $\omega = \infty$) it has been reported that the π^+/π^- ratios can be described by[42]

$$\frac{N_p^+}{N_p^-} \approx \left(\frac{N_n^+}{N_n^-}\right)^{-1} \approx 1.2 \qquad (23)$$

Clearly in electroproduction the isospin symmetry of this relationship breaks down.

One possible explanation for the π^+/π^- asymmetry in electroproduction is provided by the quark-parton model. In this model the natural variable for describing N^+/N^- variations is ω, which selects which partons within the nucleon are being struck. Some predictions from this model for N_p^+/N_p^- and N_n^+/N_n^- based on a 1-parameter fit to the former are shown in Fig. 12.[17]

Another test of the quark-parton model is provided by the sum rule in expression (17). Integrating over the range $0.4 < x < 0.85$ to define the N's and over $3 < \omega < 60$ we compute $D = 0.24 \pm 0.28$. While this is consistent with the predicted value (0.29) the errors are too large to make this a serious test.

The charge in the region $x > 0.1$, calculated using the values for N^+ and N^- in Table X, is shown as a function of ω in Fig. 13. We also show the average charge of the struck parton using the quark-parton composition in a model given by McElhaney and Tuan.[43] While the amount of charge which we see is of the same order of magnitude as the charge which we expect, the detailed agreement of the ω dependence is not good,

particularly for the n target. The disagreement does not, however, reflect on the conjecture that the parton charge should be retained by the average observed hadron. This is because we do not know what x range to include as the current fragmentation region, or how to correct for spill-over from other regions. The problem is particularly graphic in the case of the n target data where the N^+/N^- ratio appears strongly x-dependent (see Table VII or VIII). If we were to include only the more limited region $0.4 < x < 0.85$ in the analysis in Fig. 13 we would get better agreement for the shape of the distributions, but the normalization would be worse because only a fraction of the current fragmentation region is included. A similar analysis based on a preliminary version of the p data has been given by Hasenfratz.[21] The forward charge is shown as a function of q^2 in Fig. 14a.

The increase of N_p^+/N_p^- with $|q^2|$ can be partly attributed to the relative decrease of the exclusive channel $\gamma^* p \to \rho^o p$. Using the known behavior of this channel[3] we have computed the contribution of π's from ρ decay to the differential multiplicities. This contribution is shown as a function of q^2 in Table XI. Using the data in Tables X and XI we have computed the particle ratio N_p^+/N_p^- with and without the ρ contribution. This is shown as a function of q^2 in Fig. 14b. While the elastic ρ^o channel appears to account for some of the effect for $|q^2| < 0.5$ (GeV/c), it does not explain the whole effect.

That the removal of the ρ^o channel cannot explain the growing charge asymmetry can be seen in other ways. This channel cannot contribute to the forward charge $(N_p^+ - N_p^-)$, yet in Fig. 14a this charge appears to grow with $|q^2|$. Furthermore, the removal of $\gamma^* n \to \rho^o n$ from the neutron target cannot make N_n^+/N_n^- grow larger than 1, as appears to be the case.

V Conclusions

We have observed hadrons electroproduced in the direction of the virtual photon, and have studied the behavior of these hadrons in the transition region between photoproduction and leptonic scaling. A number of trends within the data are noted.

1. The cross sections are consistent with having no φ dependence for $x < 0.4$, and with having small $\cos\varphi$ and $\cos 2\varphi$ dependences for $x > 0.4$.

2. A slight broadening of the $p_\perp^2$ distributions is noted for hadrons with $x > 0.4$ as $|q^2|$ increased.

3. We observe hadronic scaling in that the structure function $f(x)$ shows no significant s (q^2) dependence at fixed ω. Furthermore, roughly the same $f(x)$ distribution is seen in all electrproduction experiments, and in photoproduction when the π's from ρ^o decay are removed.

4. The observed hadrons are less h^+/h^- symmetric in electroproduction than in photoproduction, both for the p and the n target. The nature of these asymmetries is consistent with predictions of the quark-parton model. The breakdown of relationship (24) in electroproduction precludes the validity of any model for reaction (5) which involves only a single isospin channel. The asymmetries increase with $|q^2|$, and can only partly be attributed to the decreasing role of the channel $\gamma^*N \to \rho^o N$.

ACKNOWLEDGMENTS

We wish to acknowledge the technical support contributed by numerous SLAC groups, particularly the cooperation from Steve St. Lorant and the Low Temperature group, and John Brown and the Data Analysis group.

William L. Lakin, Eric W. Petraske, Byron Dieterle and Benson T. Chertok provided valuable assistance in the early stages of the experiment.

We are indebted to W. Atwood and S. Stein for supplying us with computer programs for the evaluation of radiative corrections. We have profitted from numerous discussions with members of the SLAC Theory group.

References

1. For summaries of the experimental status of deep inelastic electron scattering see talk given by H. Kendall in Proceedings of the Fifth International Symposium on Electron and Photon Interactions at High Energies, Ithaca, New York, 1971, edited by N.B. Mistry (Cornell University Press, Ithaca, New York, 1972), and talk by E. Bloom in Proceedings of the Sixth International Symposium on Electron and Photon Interactions at High Energies, Bonn, Germany, 1973 (to be published).

2. J.T. Dakin, G.J. Feldman, W.L. Lakin, F. Martin, M.L. Perl, E.W. Petraske, and W.T. Toner, Phys. Rev. Letters 29, 746 (1972); J.T. Dakin, G.J. Feldman, F. Martin, M.L. Perl, and W.T. Toner, Phys. Rev. Letters 31, 786 (1973).

3. J.T. Dakin, G.J. Feldman, W.L. Lakin, F. Martin, M.L. Perl, E.W. Petraske, and W.T. Toner, Phys. Rev. Letters 30, 142 (1973), and Phys. Rev. D8, 687 (1973)

4. L.N. Hand, Phys. Rev. 129, 1834 (1963).

5. This variable x is the variable suggested by Feynman (Phys. Rev. Lett. 23, 1415 (1969)) for use in analyzing inclusive reactions. It should not be confused with the common usage of the symbol to represent the leptonic scaling variable.

6. J.T. Dakin, G.J. Feldman, W.L. Lakin, F. Martin, M.L. Perl, E.W. Petraske, W.T. Toner, Stanford Linear Accelerator Report No. SLAC-PUB-1074 (1972) (unpublished).

7. For summaries of the theoretical ideas related to inelastic electron scattering see F.J. Gilman, Lectures presented at the Summer Institute on Particle Interactions at Very High Energies, Louvain, Belguim (1973), SLAC Report No. SLAC-PUB-1338 (unpublished).

8. F. Ravndal, Phys. Lett. 43B, 301 (1973).

9. H. Cheng and T.T. Wu, Phys. Rev. Letters 22, 1409 (1969); J.D. Bjorken, J.B. Kogut, and D.E. Soper, Phys. Rev. D3, 1382 (1971).

10. J.B. Kogut, Phys. Rev. D5, 1152 (1972), H.D.I. Abarbanel and J.B. Kogut, Phys. Rev. D5, 2050 (1972).

11. R. Gatto and G. Preparata, Phys. Rev. D9 (to be published).

12. S.D. Drell and T.M. Yan, Phys. Rev. Letters 24, 855 (1970); E.W. Colglazier and F. Ravndal, Phys. Rev. D7, 1537 (1973).

13. J.D. Bjorken and J. Kogut, Phys. Rev. D8, 1341 (1973); J. Kogut, Phys. Rev. D8, 3029 (1973). Also see Reference 11.

14. See, for instance, T.T. Chou and C.N. Yang, Phys. Rev. D4, 2005 (1971). R.C. Hwa and C.S. Lam, Phys. Rev. D4, 2865 (1971).

15. M. Greco, CERN Report No. TH. 1617-CERN (1973).

16. C.F.A. Pantin, Nucl. Phys. B46, 205 (1972).

17. J.T. Dakin and G.J. Feldman, Phys. Rev. D8, 2862 (1973).

18. J. Cleymans and R. Rodenberg, Phys. Rev. D, (to be published).

19. M. Fronau, F. Ravndal, and Y. Zermi, Nucl. Phys. B51, 611 (1973).

20. R.P. Feynman, Photon-Hadron Interactions, W.A. Benjamin, New York, 1972.

21. P. Hasenfratz, Phys. Lett. 47B, 60 (1973).

22. G.R. Farrar and J.L. Rosner, Phys. Rev. D7, 2747 (1973).

23. R.N. Cahn and E.W. Colglazier, Stanford Linear Accelerator Report No. SLAC-PUB-1267 (1973).

24. V. Eckardt, H.J. Gebauer, P. Joos, H. Meyer, B. Naroska, D. Notz, W.J. Podolsky, G. Wolfe, S. Yellin, H. Dau, G. Drews, D. Greubel, W. Meincke, H. Nagel, and E. Rabe, Nucl. Phys. B55, 45 (1973), and Contribution to the Sixth International Symposium on Electron and Photon Interactions at High Energies, Bonn, Germany, 1973.

25. J. Ballam, E.D. Bloom, J.T. Carroll, G.B. Chadwick, R.L.A. Cottrell, M. Della Negra, H. DeStaebler, L.K. Gershwin, L.P. Keller, M.D. Mestayer, K.C. Moffeit, C.Y. Prescott, and S. Stein, Contribution to the Sixth International Symposium on Electron and Photon Interactions at High Energie, Bonn Germany, 1973; and M. Della Negra, Proceedings of the International Conference on New Results from Experiments on High Energy Particle Collisions, Vanderbilt University, April, 1973, edited by R.S. Panvini (American Institute of Physics, New York, 1973).

26. I. Dammann, C. Driver, K. Heinloth, G. Hofmann, F. Janata, P. Karow, G. Luke, D. Schmidt, and G. Specht, Nucl. Phys. B54, 381 (1973).

27. J.C. Alder, F.W. Brasse, E. Chazelas, W. Fehrenbach, W. Flauger, K.H. Frank, E. Ganssauge, J. Gayler, V. Korbel, W. Krechlok, J. May, M. Merkwitz, P.D. Zimmerman, Nucl. Phys. B46, 415 (1972).

28. C.J. Bebek, C.N. Brown, C.A. Lichtenstein, M. Herlinger, F.M. Pipkin, L.K. Sisterson, D. Andrews, K. Berkelman, D.G. Cassel, and D.L. Hartill, Phys. Rev. Lett. 30, 624 (1973) and Contributions to the Sixth International Symposium on Electron and Photon Interactions at High Energies, Bonn, Germany, 1973.

29. C.J. Bebek, C.N. Brown, M. Herzlinger, C.A. Lichtenstein, F.M. Pipkin L.K. Sisterson, D. Andres, K. Berkelman, D.G. Cassel, and D.L. Hartill, Phys. Rev. Lett. 32, 27 (1973).

30. C.J. Bebek, C.N. Brown, M. Herzlinger, S. Holmes, C.A. Lichtenstein, F.M. Pipkin, L.K. Sisterson, D. Andrews, K. Berkelman, D.G. Cassel, D.L. Hartill, N. Hicks, Phys. Rev. Lett. 32, 21 (1973).

31. E. Lazarus, D. Andrews, K. Berkelman, G. Brown, D.G. Cassel, W.R. Francis, D.L. Hartill, J. Hartmann, R.M. Littauer, R.L. Loveless, R.C. Rohlfs, D.H. White and A.J. Sadoff, Phys. Rev. Lett. 29, 743 (1972); Phys. Rev. Lett. 29, 1409 (1972); Phys. Rev. D (to be published); and D.L. Hartill, Proceedings of the International Conference on New Results from Experiments on High Energy Particle Collisions, Vanderbilt University, April, 1973, edited by R.S. Panvini (American Institute of Physics, New York, 1973).

32. F. Martin, S.J. St. Lorant, and W.T. Toner, Nucl. Instrum. Methods 103, 503 (1972); A.C. Newton, F. Martin, S.J. St. Lorant, and W.T. Toner, Rev. Sci. Instrum. 44, 244 (1973); F. Martin and S.J. St. Lorant, J. Appl. Phys. 44, 460 (1973).

33. W.L. Lakin, E.W. Petraske, and W.T. Toner, Nucl. Instrum. Methods 103, 431 (1972).

34. W.L. Lakin and R.E. Baggs, Nucl. Instrum. Methods 102, 267 (1972).

35. J.L. Brown, SLAC Report No. SLAC-PUB-752, (1970) (unpublished).

36. G. Miller, SLAC Report No. SLAC-PUB-129 (1971) (unpublished).

37. A. Bodek, Massachusetts Institute of Technology, Laboratory for Nuclear Science Technical Report No. COO-3060-116 (1972).

38. A. Bodek, M. Breidenbach, D.L. Dubin, J.E. Elias, J.I. Friedman, H.W. Kendall, J.S. Pouncher, E.M. Riordan, M.R. Sogard, and D.H. Coward, Phys. Rev. Lett. 30, 1087 (1973); D.O. Caldwell, V.B. Elings, W.P. Hesse, R.J. Morrison, F.V. Murphy, and D.E. Yount, Phys. Rev. D7, 1362 (1973).

39. H. Burfeindt, G. Buschhorn, H. Genzel, P. Heide, U. Kotz, K.-H. Me , P. Schmuser, B. Sonne, G. Vogel and B.H. Wiik, contribution to the VI International Symposium on Electron and Photon Interactions at High Energies, Bonn, Germany, 1973.

40. A.M. Boyarski, D. Coward, S. Ecklund, B. Richter, D. Sherden, R. Siemann, and C. Sinclair, contribution to the International Symposium On Electron and Photon Interactions at High Energy, Ithaca, New York, (1971), and private communication.

41. K.C. Moffeit, J. Ballam, G.B. Chadwick, M. Della-Negra, R. Gearhart, J.J. Murray, P. Seyboth, C.K. Sinclair, I.O. Skillicorn, H. Spitzer, G. Wolf, and H.H. Bingham, W.B. Fretter, W.J. Podolsky, M.S. Rabin, A.H. Rosenfeld, R. Windmolders, G.P. Yost, and R.H. Milburn, Phys. Rev. D5, 1603 (1972), and private communication.

42. J. Gandsman, G. Alexander, S. Dagan, L.D. Jacobs, A. Levy, D. Lissauer and L.M. Rosenstein, Nucl. Phys. B61, 32 (1973).

43. R. McElhaney and S.F. Tuan, Phys. Rev. D8, 2267 (1973).

Table I

Kinematic range of experiment

Variable	Range
q^2	-0.25 to -3.0 $(GeV/c)^2$
s	12 to 30 GeV^2
$p_\perp^2$	0.0 to 0.7 GeV^2
ϕ	0 to 2π
x	0.1 to 1.0

Table II

Data Samples

	Target	
	H_2	D_2
Incident electrons	2.6×10^{12}	0.7×10^{12}
Triggers	2.5×10^5	1.1×10^5
e' events	30401	14772
e'-h events	9250	4663

Table III

Scanning-Measuring Efficiencies

	Data Sample	
Event type	H_2	D_2
e'	.805	.787
e' h^-	.543	.505
e' h^+	.579	.539

Table IV

Proton Contamination in h^+ Spectrum

	dN/dx	
X range	Observed	Proton Contamination (See text)
0.1 to 0.25	3.52 ± 0.11	.35
0.25 to 0.40	1.42 ± 0.04	.10
0.40 to 0.55	0.70 ± 0.03	.035
0.55 to 0.70	0.34 ± 0.02	.020
0.70 to 0.85	0.19 ± 0.01	.010
0.85 to 1.00	0.11 ± 0.01	.005

TABLE V

Transverse Momentum and Azimuthal Angle Parameters in q^2 - s Regions

tgt.	had.	s GeV^2	q2 $(GeV/c)^2$	0.1<x<0.4 b $(c/GeV)^2$	0.1<x<0.4 A	0.1<x<0.4 B	0.4<x<1.0 b $(c/GeV)^2$	0.4<x<1.0 A	0.4<x<1.0 B
p	h-	12-30	.25-0.5	6.3+-0.3	0.10+-0.05	0.13+-0.05	6.5+-0.4	0.18+-0.08	0.03+-0.07
p	h-	12-30	0.5-1.0	6.7+-0.3	0.08+-0.04	0.03+-0.04	6.4+-0.3	0.23+-0.07	0.15+-0.07
p	h-	12-30	1.0-2.0	6.7+-0.4	0.08+-0.06	0.05+-0.06	5.1+-0.4	0.00+-0.09	0.08+-0.09
p	h-	12-30	2.0-3.0	7.0+-0.9	0.18+-0.12	-0.03+-0.13	4.8+-1.0	0.28+-0.23	0.08+-0.30
p	h-	12-18	0.5-3.0	6.2+-0.4	0.08+-0.06	0.03+-0.05	5.8+-0.4	0.15+-0.08	0.00+-0.08
p	h-	18-24	0.5-3.0	6.8+-0.4	0.10+-0.06	0.00+-0.05	5.8+-0.4	0.13+-0.09	0.23+-0.08
p	h-	24-30	0.5-3.0	7.7+-0.5	0.10+-0.07	0.08+-0.07	6.3+-0.6	0.35+-0.15	0.20+-0.12
p	h+	12-30	.25-0.5	6.0+-0.3	-0.08+-0.04	-0.10+-0.04	5.6+-0.3	0.13+-0.06	0.08+-0.05
p	h+	12-30	0.5-1.0	6.0+-0.2	0.00+-0.03	-0.08+-0.04	5.0+-0.2	0.13+-0.05	0.08+-0.05
p	h+	12-30	1.0-2.0	5.5+-0.3	-0.05+-0.05	0.00+-0.05	4.1+-0.3	0.05+-0.07	0.03+-0.07
p	h+	12-30	2.0-3.0	5.6+-0.6	-0.15+-0.10	0.15+-0.10	3.4+-0.5	-0.08+-0.13	-0.03+-0.13
p	h+	12-18	0.5-3.0	5.2+-0.3	-0.10+-0.04	-0.05+-0.04	4.4+-0.3	0.10+-0.06	-0.10+-0.06
p	h+	18-24	0.5-3.0	5.8+-0.3	0.03+-0.05	0.00+-0.04	4.5+-0.3	0.10+-0.07	0.10+-0.06
p	h+	24-30	0.5-3.0	6.8+-0.4	0.03+-0.06	0.00+-0.06	5.2+-0.4	0.27+-0.11	0.35+-0.08
d	h-	12-30	.25-0.5	6.3+-0.5	0.13+-0.07	-0.03+-0.07	5.9+-0.5	0.15+-0.11	0.17+-0.10
d	h-	12-30	0.5-1.0	5.2+-0.4	-0.05+-0.06	-0.03+-0.06	5.3+-0.4	0.18+-0.10	0.15+-0.09
d	h-	12-30	1.0-2.0	7.1+-0.6	0.03+-0.08	-0.05+-0.08	5.5+-0.6	-0.10+-0.13	0.08+-0.12
d	h-	12-30	2.0-3.0	7.2+-0.8	-0.03+-0.17	0.05+-0.18	4.7+-1.0	0.20+-0.24	-0.20+-0.22
d	h-	12-18	0.5-3.0	6.1+-0.5	-0.03+-0.08	0.10+-0.07	6.3+-0.6	0.15+-0.12	0.15+-0.11
d	h-	18-24	0.5-3.0	5.3+-0.4	-0.10+-0.07	-0.08+-0.07	4.8+-0.5	-0.03+-0.12	0.13+-0.12
d	h-	24-30	0.5-3.0	6.6+-0.6	0.18+-0.09	-0.20+-0.10	4.6+-0.8	0.25+-0.22	-0.13+-0.17
d	h+	12-30	.25-0.5	7.1+-0.4	0.03+-0.06	0.05+-0.06	6.0+-0.4	0.23+-0.08	0.15+-0.07
d	h+	12-30	0.5-1.0	7.0+-0.4	0.03+-0.06	0.05+-0.05	4.5+-0.3	0.15+-0.07	-0.05+-0.07
d	h+	12-30	1.0-2.0	5.9+-0.4	-0.05+-0.07	-0.03+-0.06	4.1+-0.4	0.08+-0.10	0.05+-0.10
d	h+	12-30	2.0-3.0	4.6+-0.8	-0.05+-0.15	0.18+-0.17	3.9+-0.9	-0.28+-0.19	0.13+-0.20
d	h+	12-18	0.5-3.0	5.9+-0.4	-0.08+-0.07	0.05+-0.06	4.6+-0.4	0.08+-0.08	-0.03+-0.08
d	h+	18-24	0.5-3.0	6.5+-0.4	0.08+-0.07	0.05+-0.07	4.0+-0.4	0.10+-0.09	0.00+-0.09
d	h+	24-30	0.5-3.0	7.1+-0.6	-0.03+-0.08	-0.03+-0.08	4.2+-0.6	0.13+-0.16	-0.03+-0.12

TABLE VI

Transverse Momentum and Azimuthal Angle Parameters Versus x

tgt.	had.	s GeV^2	q^2 $(GeV/c)^2$	x	b $(c/GeV)^2$	A	B	dN/dx
p	h-	12-30	0.5-3.0	0.10-0.25	6.1+-0.3	0.02+-0.04	0.03+-0.04	2.46+-0.08
p	h-	12-30	0.5-3.0	0.25-0.40	6.0+-0.3	0.05+-0.05	-0.08+-0.06	0.89+-0.04
p	h-	12-30	0.5-3.0	0.40-0.55	5.1+-0.4	0.03+-0.08	0.00+-0.02	0.39+-0.02
p	h-	12-30	0.5-3.0	0.55-0.70	5.3+-0.5	0.13+-0.11	0.13+-0.11	0.19+-0.01
p	h-	12-30	0.5-3.0	0.70-0.85	6.7+-0.7	0.13+-0.13	0.03+-0.12	0.12+-0.01
p	h-	12-30	0.5-3.0	0.85-1.00	9.0+-0.6	0.05+-0.18	0.43+-0.07	0.06+-0.01
p	h+	12-30	0.5-3.0	0.10-0.25	5.2+-0.3	-0.08+-0.03	-0.03+-0.03	3.52+-0.11
p	h+	12-30	0.5-3.0	0.25-0.40	5.3+-0.2	-0.03+-0.04	-0.08+-0.04	1.42+-0.04
p	h+	12-30	0.5-3.0	0.40-0.55	4.6+-0.3	0.13+-0.06	0.05+-0.06	0.70+-0.03
p	h+	12-30	0.5-3.0	0.55-0.70	4.3+-0.3	-0.25+-0.08	0.00+-0.08	0.34+-0.02
p	h+	12-30	0.5-3.0	0.70-0.85	3.9+-0.4	0.00+-0.10	-0.13+-0.10	0.19+-0.01
p	h+	12-30	0.5-3.0	0.85-1.00	5.1+-0.6	0.15+-0.13	0.08+-0.12	0.11+-0.01
d	h-	12-30	0.5-3.0	0.10-0.25	5.4+-0.4	-0.03+-0.06	-0.15+-0.06	2.65+-0.14
d	h-	12-30	0.5-3.0	0.25-0.40	5.2+-0.4	-0.08+-0.07	0.05+-0.07	1.11+-0.06
d	h-	12-30	0.5-3.0	0.40-0.55	5.4+-0.5	0.08+-0.11	0.03+-0.11	0.40+-0.03
d	h-	12-30	0.5-3.0	0.55-0.70	4.3+-0.6	0.05+-0.16	0.18+-0.14	0.21+-0.02
d	h-	12-30	0.5-3.0	0.70-0.85	5.1+-0.8	-0.25+-0.17	-0.18+-0.18	0.15+-0.02
d	h-	12-30	0.5-3.0	0.85-1.00	9.0+-1.0	0.18+-0.24	0.15+-0.23	0.06+-0.01
d	h+	12-30	0.5-3.0	0.10-0.25	5.4+-0.4	-0.03+-0.05	-0.02+-0.05	3.50+-0.15
d	h+	12-30	0.5-3.0	0.25-0.40	6.1+-0.4	-0.05+-0.06	0.05+-0.06	1.33+-0.06
d	h+	12-30	0.5-3.0	0.40-0.55	4.3+-0.3	0.13+-0.08	-0.05+-0.08	0.71+-0.04
d	h+	12-30	0.5-3.0	0.55-0.70	4.0+-0.5	0.03+-0.11	-0.15+-0.11	0.35+-0.03
d	h+	12-30	0.5-3.0	0.70-0.85	4.1+-0.6	-0.35+-0.13	0.05+-0.12	0.23+-0.02
d	h+	12-30	0.5-3.0	0.85-1.00	5.1+-1.0	0.15+-0.22	0.03+-0.22	0.08+-0.01

TABLE VII

f(x) as a Function of q^2 and x

tgt.	had.	s GeV^2	q^2 $(GeV/c)^2$	f(x) 0.10<x<0.25	0.25<x<0.40	0.40<x<0.55	0.55<x<0.70	0.70<x<0.85	0.85<x<1.00
p	h-	12-30	.25-0.5	0.190+-0.012	0.107+-0.007	0.080+-0.006	0.057+-0.006	0.039+-0.005	0.021+-0.004
p	h+	12-30	.25-0.5	0.260+-0.015	0.161+-0.008	0.118+-0.007	0.101+-0.007	0.074+-0.007	0.038+-0.005
d	h-	12-30	.25-0.5	0.233+-0.019	0.114+-0.012	0.081+-0.009	0.077+-0.009	0.034+-0.007	0.021+-0.006
d	h+	12-30	.25-0.5	0.229+-0.016	0.170+-0.011	0.125+-0.010	0.107+-0.011	0.051+-0.008	0.040+-0.008
n	h-	12-30	.25-0.5	0.285+-0.039	0.123+-0.024	0.082+-0.019	0.100+-0.020	0.027+-0.015	0.022+-0.013
n	h+	12-30	.25-0.5	0.194+-0.035	0.182+-0.024	0.135+-0.022	0.115+-0.023	0.023+-0.018	0.042+-0.017
p	h-	12-30	0.5-1.0	0.219+-0.011	0.112+-0.006	0.068+-0.005	0.043+-0.004	0.034+-0.004	0.021+-0.003
p	h+	12-30	0.5-1.0	0.309+-0.014	0.172+-0.007	0.116+-0.006	0.074+-0.005	0.046+-0.005	0.036+-0.004
d	h-	12-30	0.5-1.0	0.261+-0.021	0.150+-0.011	0.063+-0.007	0.047+-0.006	0.043+-0.006	0.022+-0.005
d	h+	12-30	0.5-1.0	0.266+-0.017	0.163+-0.010	0.130+-0.010	0.087+-0.008	0.057+-0.007	0.023+-0.005
n	h-	12-30	0.5-1.0	0.313+-0.043	0.195+-0.022	0.057+-0.014	0.051+-0.013	0.056+-0.013	0.024+-0.010
n	h+	12-30	0.5-1.0	0.214+-0.037	0.153+-0.020	0.147+-0.021	0.102+-0.017	0.072+-0.015	0.008+-0.010
p	h-	12-30	1.0-2.0	0.189+-0.013	0.099+-0.007	0.061+-0.006	0.043+-0.006	0.027+-0.004	0.017+-0.004
p	h+	12-30	1.0-2.0	0.310+-0.020	0.191+-0.010	0.127+-0.009	0.070+-0.008	0.051+-0.007	0.032+-0.005
d	h-	12-30	1.0-2.0	0.183+-0.016	0.113+-0.011	0.072+-0.009	0.034+-0.007	0.027+-0.006	0.019+-0.006
d	h+	12-30	1.0-2.0	0.392+-0.031	0.156+-0.012	0.111+-0.012	0.060+-0.009	0.061+-0.010	0.028+-0.007
n	h-	12-30	1.0-2.0	0.176+-0.034	0.131+-0.023	0.086+-0.019	0.022+-0.015	0.026+-0.013	0.022+-0.012
n	h+	12-30	1.0-2.0	0.496+-0.064	0.112+-0.027	0.092+-0.025	0.047+-0.020	0.074+-0.021	0.023+-0.015
p	h-	12-30	2.0-3.0	0.185+-0.031	0.118+-0.016	0.047+-0.012	0.024+-0.008	0.026+-0.009	0.010+-0.006
p	h+	12-30	2.0-3.0	0.314+-0.046	0.173+-0.023	0.121+-0.017	0.085+-0.016	0.068+-0.015	0.032+-0.011
d	h-	12-30	2.0-3.0	0.189+-0.037	0.117+-0.023	0.062+-0.017	0.056+-0.019	0.050+-0.019	0.014+-0.010
d	h+	12-30	2.0-3.0	0.265+-0.052	0.201+-0.033	0.128+-0.027	0.077+-0.021	0.065+-0.021	0.007+-0.007
n	h-	12-30	2.0-3.0	0.194+-0.080	0.115+-0.048	0.082+-0.037	0.099+-0.039	0.082+-0.039	0.020+-0.021
n	h+	12-30	2.0-3.0	0.196+-0.114	0.239+-0.070	0.135+-0.056	0.065+-0.046	0.061+-0.044	-.026+-0.018

TABLE VIII

dN/dx as a Function of q^2 and x

tgt.	had.	s GeV^2	q^2 $(GeV/c)^2$	dN/dx 0.10<x<0.25	0.25<x<0.40	0.40<x<0.55	0.55<x<0.70	0.70<x<0.85	0.85<x<1.00
p	h-	12-30	.25-0.5	2.416+-0.124	0.893+-0.055	0.503+-0.037	0.279+-0.028	0.158+-0.022	0.073+-0.015
p	h+	12-30	.25-0.5	3.017+-0.136	1.301+-0.061	0.702+-0.042	0.477+-0.034	0.287+-0.026	0.124+-0.018
d	h-	12-30	.25-0.5	2.920+-0.206	0.939+-0.084	0.499+-0.055	0.375+-0.047	0.139+-0.030	0.074+-0.021
d	h+	12-30	.25-0.5	2.855+-0.174	1.404+-0.092	0.754+-0.062	0.506+-0.051	0.196+-0.032	0.132+-0.026
n	h-	12-30	.25-0.5	3.527+-0.431	0.998+-0.176	0.498+-0.116	0.489+-0.097	0.116+-0.063	0.075+-0.045
n	h+	12-30	.25-0.5	2.676+-0.374	1.531+-0.193	0.818+-0.131	0.543+-0.107	0.090+-0.068	0.141+-0.056
p	h-	12-30	0.5-1.0	2.644+-0.114	0.947+-0.048	0.414+-0.029	0.208+-0.019	0.133+-0.015	0.069+-0.011
p	h+	12-30	0.5-1.0	3.491+-0.132	1.383+-0.056	0.687+-0.036	0.347+-0.024	0.175+-0.017	0.117+-0.013
d	h-	12-30	0.5-1.0	2.866+-0.198	1.225+-0.082	0.381+-0.049	0.223+-0.030	0.173+-0.025	0.073+-0.016
d	h+	12-30	0.5-1.0	3.155+-0.172	1.339+-0.077	0.758+-0.056	0.402+-0.038	0.222+-0.027	0.076+-0.015
n	h-	12-30	0.5-1.0	3.141+-0.412	1.561+-0.172	0.344+-0.084	0.242+-0.063	0.221+-0.052	0.078+-0.033
n	h+	12-30	0.5-1.0	2.761+-0.368	1.289+-0.163	0.844+-0.118	0.470+-0.080	0.279+-0.057	0.027+-0.033
p	h-	12-30	1.0-2.0	2.260+-0.139	0.812+-0.056	0.371+-0.036	0.202+-0.029	0.108+-0.017	0.056+-0.012
p	h+	12-30	1.0-2.0	3.424+-0.189	1.494+-0.078	0.733+-0.052	0.320+-0.032	0.195+-0.025	0.105+-0.016
d	h-	12-30	1.0-2.0	2.279+-0.187	0.933+-0.087	0.430+-0.055	0.160+-0.033	0.107+-0.025	0.063+-0.018
d	h+	12-30	1.0-2.0	4.135+-0.306	1.268+-0.098	0.655+-0.067	0.274+-0.047	0.233+-0.041	0.092+-0.024
n	h-	12-30	1.0-2.0	2.302+-0.400	1.083+-0.183	0.524+-0.115	0.108+-0.072	0.106+-0.052	0.071+-0.038
n	h+	12-30	1.0-2.0	5.021+-0.641	0.986+-0.211	0.557+-0.143	0.216+-0.098	0.280+-0.085	0.075+-0.050
p	h-	12-30	2.0-3.0	2.177+-0.295	0.978+-0.132	0.293+-0.083	0.116+-0.039	0.105+-0.035	0.034+-0.020
p	h+	12-30	2.0-3.0	3.408+-0.399	1.359+-0.156	0.714+-0.100	0.526+-0.163	0.291+-0.084	0.106+-0.038
d	h-	12-30	2.0-3.0	2.287+-0.408	0.974+-0.189	0.384+-0.107	0.262+-0.090	0.217+-0.092	0.048+-0.034
d	h+	12-30	2.0-3.0	2.290+-0.490	1.569+-0.318	0.740+-0.154	0.357+-0.097	0.261+-0.091	0.041+-0.043
n	h-	12-30	2.0-3.0	2.421+-0.868	0.965+-0.401	0.500+-0.229	0.452+-0.184	0.363+-0.188	0.065+-0.070
n	h+	12-30	2.0-3.0	2.225+-1.057	1.836+-0.654	0.770+-0.323	0.135+-0.254	0.221+-0.200	-.044+-0.093

TABLE IX

f(x) as a Function of s at Fixed ω

tgt.	had.	s GeV^2	ω	f(x)					
				0.10<x<0.25	0.25<x<0.40	0.40<x<0.55	0.55<x<0.70	0.70<x<0.85	0.85<x<1.00
p	h-	12-18	10-35	0.263+-0.023	0.111+-0.008	0.071+-0.006	0.045+-0.005	0.032+-0.004	0.023+-0.004
p	h-	18-24	10-35	0.193+-0.013	0.111+-0.009	0.071+-0.007	0.041+-0.006	0.033+-0.005	0.020+-0.004
p	h-	24-30	10-35	0.219+-0.022	0.082+-0.012	0.069+-0.012	0.034+-0.009	0.010+-0.006	0.012+-0.007
p	h+	12-18	10-35	0.409+-0.049	0.198+-0.014	0.126+-0.009	0.074+-0.006	0.049+-0.006	0.029+-0.004
p	h+	18-24	10-35	0.328+-0.024	0.170+-0.010	0.122+-0.009	0.077+-0.008	0.054+-0.008	0.033+-0.005
p	h+	24-30	10-35	0.324+-0.039	0.166+-0.016	0.104+-0.014	0.074+-0.015	0.056+-0.014	0.049+-0.017

TABLE X
Multiplicities and Particle Ratios

tgt.	s GeV^2	q^2 or ω	0.1<x<1.0 N-	0.1<x<1.0 N+	0.1<x<1.0 N+/N-	0.4<x<0.85 N-	0.4<x<0.85 N+	0.4<x<0.85 N+/N-
p	12-30	$0.25<q^2<0.50$	0.648+-0.021	0.888+-0.024	1.37+-0.06	0.140+-0.008	0.219+-0.009	1.56+-0.11
n	12-30	$0.25<q^2<0.50$	0.855+-0.074	0.870+-0.069	1.02+-0.12	0.165+-0.024	0.218+-0.027	1.32+-0.26
p	12-30	$0.50<q^2<1.00$	0.662+-0.020	0.930+-0.023	1.40+-0.05	0.113+-0.006	0.182+-0.007	1.60+-0.10
n	12-30	$0.50<q^2<1.00$	0.838+-0.069	0.850+-0.065	1.01+-0.11	0.121+-0.018	0.239+-0.023	1.97+-0.34
p	12-30	$1.00<q^2<2.00$	0.571+-0.024	0.941+-0.032	1.65+-0.09	0.102+-0.007	0.187+-0.010	1.83+-0.16
n	12-30	$1.00<q^2<2.00$	0.629+-0.070	1.070+-0.106	1.70+-0.25	0.111+-0.022	0.158+-0.029	1.43+-0.39
p	12-30	$2.00<q^2<3.00$	0.556+-0.051	0.961+-0.072	1.73+-0.20	0.077+-0.015	0.230+-0.031	2.98+-0.70
n	12-30	$2.00<q^2<3.00$	0.715+-0.153	0.772+-0.199	1.08+-0.36	0.197+-0.052	0.170+-0.069	0.86+-0.42
p	12-18	$0.25<q^2<3.00$	0.620+-0.023	0.969+-0.030	1.56+-0.08	0.108+-0.006	0.191+-0.008	1.77+-0.12
n	12-18	$0.25<q^2<3.00$	0.585+-0.063	0.939+-0.090	1.61+-0.23	0.113+-0.017	0.205+-0.023	1.81+-0.34
p	18-24	$0.25<q^2<3.00$	0.631+-0.019	0.899+-0.021	1.43+-0.06	0.119+-0.005	0.202+-0.008	1.71+-0.11
n	18-24	$0.25<q^2<3.00$	0.916+-0.070	0.777+-0.063	0.85+-0.09	0.159+-0.020	0.180+-0.023	1.13+-0.20
p	24-30	$0.25<q^2<3.00$	0.646+-0.023	0.909+-0.026	1.41+-0.06	0.125+-0.009	0.187+-0.010	1.49+-0.13
n	24-30	$0.25<q^2<3.00$	0.804+-0.075	1.036+-0.080	1.29+-0.16	0.123+-0.026	0.252+-0.032	2.05+-0.51
p	12-30	$3 < \omega < 10$	0.567+-0.047	0.858+-0.049	1.51+-0.15	0.078+-0.010	0.191+-0.019	2.46+-0.41
n	12-30	$3 < \omega < 10$	0.520+-0.113	0.756+-0.151	1.46+-0.43	0.157+-0.036	0.125+-0.046	0.80+-0.35
p	12-30	$10 < \omega < 20$	0.607+-0.025	0.965+-0.033	1.59+-0.09	0.107+-0.007	0.183+-0.009	1.71+-0.14
n	12-30	$10 < \omega < 20$	0.776+-0.080	1.034+-0.111	1.33+-0.20	0.123+-0.022	0.180+-0.027	1.47+-0.34
p	12-30	$20 < \omega < 35$	0.656+-0.024	0.960+-0.032	1.46+-0.07	0.116+-0.007	0.194+-0.009	1.68+-0.12
n	12-30	$20 < \omega < 35$	0.729+-0.077	0.840+-0.082	1.15+-0.17	0.110+-0.025	0.206+-0.026	1.88+-0.43
p	12-30	$35 < \omega < 60$	0.670+-0.025	0.957+-0.029	1.43+-0.07	0.140+-0.009	0.211+-0.010	1.51+-0.12
n	12-30	$35 < \omega < 60$	0.955+-0.086	0.830+-0.082	0.87+-0.12	0.170+-0.028	0.246+-0.032	1.44+-0.31
p	12-18	$10 < \omega < 35$	0.653+-0.029	0.973+-0.042	1.49+-0.09	0.112+-0.007	0.186+-0.009	1.66+-0.13
n	12-18	$10 < \omega < 35$	0.589+-0.077	1.126+-0.143	1.91+-0.35	0.100+-0.020	0.225+-0.027	2.26+-0.53
p	18-24	$10 < \omega < 35$	0.612+-0.025	0.959+-0.034	1.57+-0.09	0.112+-0.008	0.196+-0.010	1.74+-0.16
n	18-24	$10 < \omega < 35$	0.949+-0.099	0.843+-0.098	0.89+-0.14	0.141+-0.026	0.170+-0.031	1.20+-0.31
p	24-30	$10 < \omega < 35$	0.631+-0.044	0.987+-0.058	1.57+-0.14	0.095+-0.014	0.182+-0.018	1.92+-0.34
n	24-30	$10 < \omega < 35$	0.867+-0.127	0.869+-0.152	1.30+-0.34	0.116+-0.043	0.146+-0.052	1.25+-0.64

TABLE XI

Contribution to dN/dx from Elastic Rho Decay

tgt.	had.	s GeV^2	q^2 (GeV/c)^2	dN/dx					
				0.10<x<0.25	0.25<x<0.40	0.40<x<0.55	0.55<x<0.70	0.70<x<0.85	0.85<x<1.00
p	h+,h-	12-30	.25-0.5	.078	.098	.113	.099	.079	.035
p	h+,h-	12-30	0.5-1.0	.065	.070	.077	.070	.065	.033
p	h+,h-	12-30	1.0-2.0	.047	.042	.042	.043	.047	.032
p	h+,h-	12-30	2.0-3.0	.031	.023	.021	.023	.031	.024

Figure Captions

1. One-photon-exchange diagram for reactions (1) and (2).
2. Schematic elevation view of the apparatus.
3. Geometric acceptance of the apparatus averaged over the azimuthal angle.
4. Slope parameters describing the $p_\perp^2$ distributions for (a) h^+ from hydrogen (b) h^- from hydrogen, (c) h^+ from deuterium, and (d) h^- from deuterium. The data are taken from Table V, and the points at $q^2 = 0$ are described in the text.
5. Slope parameters describing the $p_\perp^2$ distributions for the 4 reactions, plotted as a function of x. The data are from Table VI.
6. Typical structure function spectra from Table VII on a logarithmic scale.
7. Typical structure function spectra from Table VII on a linear scale. These data are the same as those in Fig. 6.
8. Differential multiplicity spectra from Table VI showing (a) the h^+ and h^- spectra, (b) the difference whose integral represents the change, and (c) the ratio.
9. A test of hadronic scaling using data from Table IX.
10. Comparison of structure functions from various electroproduction and photoproduction experiments. Included are the experiments of Moffeit et al.,[41] Bebek et al.,[28] Eckardt et al.,[24] and Ballam et al.[25]
11. Particle ratios for the region $0.4 < x < 0.85$ plotted versus q^2. Data are extracted from the work of Gandsman et al,[42] Dammann et al.,[26] Alder et al.,[27] Bebek et al.,[28] and Ballam et al.,[25] all of whom are at least partially able to reject kaons and protons, and report only pions. Data are shown for (a) proton and (b) neutron targets.
12. Particle ratios for the region $0.4 < x < 0.85$ plotted versus ω. The data points are largely the same data points as in Fig. 11, although our data has been re-binned. Data are shown for (a) proton and (b) neutron targets. The curves are taken from the quark-parton model predictions of Dakin and Feldman.[17]
13. The charge in the region $x > 0.1$ is given as a function of ω for (a) proton and (b) neutron targets. The curves represent the average charge of the struck parton in a quark parton model.
14. Plotted versus q^2 are (a) the forward charge and (b) the forward particle ratio with and without the ρ contribution. The data at $q^2 = 0$ are taken from the $s = 18.4$ GeV^2 experiment of Moffeit et al.[41]

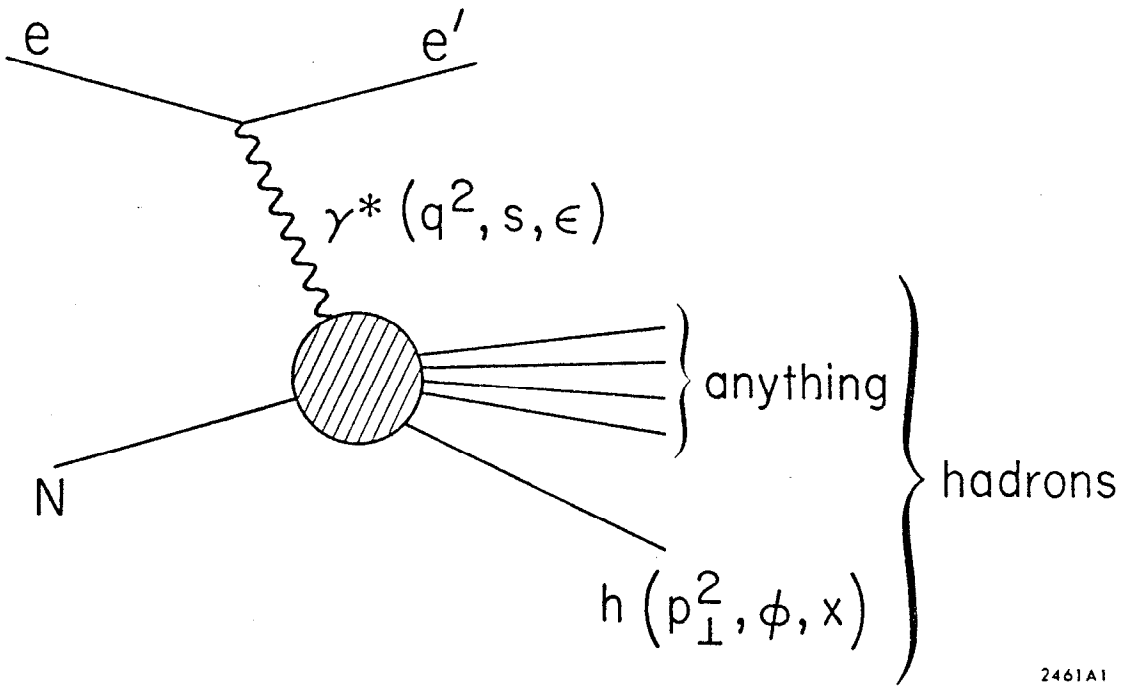

Fig. 1